Nanosecond plasma enhanced $H_2/O_2/N_2$ premixed flat flames

Sharath Nagaraja[1], Ting Li[2], Jeffrey A. Sutton[2], Igor V. Adamovich[2], Vigor Yang[1]

1. School of Aerospace Engineering, Georgia Institute of Technology, Atlanta, GA 600036

2. Department of Mechanical and Aerospace Engineering, Ohio State University, Columbus, OH 43210

Corresponding author: Sharath Nagaraja
School of Aerospace Engineering
Georgia Institute of Technology
Atlanta, GA 30332, USA
Tel: +1-404-433-0573
Email: sharath@gatech.edu

Colloquium topic: New technology

Key Words: Plasma-assisted combustion, nanosecond plasma discharge, burner stabilized premixed flame, plasma fluid modeling, Laser Induced Fluorescence, Thermometry.

Paper length (method 1):

Main Text:	word processor count	=	3660	
Equations:	(1+2)x(7.6 words/line)x1	=	31	
References:	(22+2)x(2.3 lines/reference)x(7.6 words/line)	=	420	
Figure Captions:	word processor count	=	272	
				4383
Figure 1:	(49 mm+10)x(2.2 words/mm)x(1 column)	=	130	
Figure 2:	(65 mm+10)x(2.2 words/mm)x(2 column)	=	330	
Figure 3:	(50 mm+10)x(2.2 words/mm)x(1 column)	=	132	
Figure 4:	(50 mm+10)x(2.2 words/mm)x(1 column)	=	132	
Figure 5:	(50 mm+10)x(2.2 words/mm)x(1 column)	=	132	
Figure 6a:	(50 mm+10)x(2.2 words/mm)x(1 column)	=	132	
Figure 6b:	(50 mm+10)x(2.2 words/mm)x(1 column)	=	132	
Figure 7:	(61 mm+10)x(2.2 words/mm)x(1 column)	=	157	
Figure 8:	(50 mm+10)x(2.2 words/mm)x(1 column)	=	132	
				1409
		Total	**=**	**5792 words**

Color reproduction: no (color line figures are to be printed in gray scale)
Supplementary document (none)

Report Documentation Page

Form Approved
OMB No. 0704-0188

1. REPORT DATE	2. REPORT TYPE	3. DATES COVERED
2014		**00-00-2014 to 00-00-2014**

4. TITLE AND SUBTITLE	5a. CONTRACT NUMBER
Nanosecond plasma enhanced H2/O2/N2 premixed flat flames	5b. GRANT NUMBER
	5c. PROGRAM ELEMENT NUMBER
6. AUTHOR(S)	5d. PROJECT NUMBER
	5e. TASK NUMBER
	5f. WORK UNIT NUMBER
7. PERFORMING ORGANIZATION NAME(S) AND ADDRESS(ES) **School of Aerospace Engineering,Georgia Institute of Technology,Atlanta,GA,600036**	8. PERFORMING ORGANIZATION REPORT NUMBER
9. SPONSORING/MONITORING AGENCY NAME(S) AND ADDRESS(ES)	10. SPONSOR/MONITOR'S ACRONYM(S)
	11. SPONSOR/MONITOR'S REPORT NUMBER(S)

12. DISTRIBUTION/AVAILABILITY STATEMENT
Approved for public release; distribution unlimited

13. SUPPLEMENTARY NOTES

14. ABSTRACT

15. SUBJECT TERMS

16. SECURITY CLASSIFICATION OF:			17. LIMITATION OF ABSTRACT	18. NUMBER OF PAGES	19a. NAME OF RESPONSIBLE PERSON
a. REPORT **unclassified**	b. ABSTRACT **unclassified**	c. THIS PAGE **unclassified**	**Same as Report (SAR)**	**23**	

Abstract

The effect of nanosecond pulsed plasma discharges on a laminar, lean (ϕ = 0.5) premixed $H_2/O_2/N_2$ flame is studied at low pressure (25 torr), using a novel plasma-flame facility, non-intrusive laser diagnostics, and high-fidelity numerical simulations. Spatially-resolved quantitative OH mole fraction and temperature measurements are performed with and without a burst of 200 nanosecond discharge pulses using laser-induced fluorescence. Measured temperatures increase by ~20% in both the pre-heat and post-flame zones with the use of the plasma discharge. In addition, OH mole fractions increase by 100 - 500% in the preheat zone and an average increase of 40% in the post-flame gases. Simulations are conducted with a one-dimensional, multi-scale, pulsed-discharge model with detailed plasma-combustion kinetics to develop additional insight into the complex plasma and flame interactions. Good agreement between measured and predicted OH and temperature profiles provides confidence in the model framework. The reduced electric field, E/N, during each pulse varies inversely with number density. A significant portion of the input energy is expended to electron impact ionization in the high temperature regions downstream of the flame because of high E/N in this region (700-1000 Td). Lower E/N values (100-700 Td) in the lower-temperature preheat regions, promote efficient generation of radicals and excited species via electron impact processes, as well as by collisional quenching of excited states. The plasma action results in a significant increase in O and H densities, with the peak values increasing by a factor of 6 and 4 respectively. With the plasma on, species and temperature profiles move upstream (i.e. closer to the burner) by approximately 0.2 cm. Simulations show that electron impact dissociation and excitation processes in the plasma have a major impact on the observed temperature and species profile displacement, such that Joule heating alone cannot account for it.

1. Introduction

In recent years, nonequilibrium plasma discharges have received considerable attention for enhancement of ignition and flame stabilization in a variety of combustion systems [1]. High values of local electric field to number density ratio (E/N) in nanosecond discharges [1-2], in the range of 100-1000 Td (1 Td = 10^{-17} V-cm^2) allows for efficient generation of radicals and excited species via electron impact reactions, which kinetically enhance the ignition and flame stabilization processes.

Both experimental and numerical investigations previously have been conducted to understand the role of plasma-generated species on ignition [3-6], flame speed enhancement [7], flame stabilization and extinction [8-10]. Recent studies on ignition of mildly preheated (473-500 K) H_2-air mixtures [3-4] subjected to pulsed nanosecond plane-to-plane dielectric barrier discharges demonstrated that ignition kernel growth was an order of magnitude faster than the heat transport rates. The local plasma chemistry effects brought the mixture to the ignition threshold, resulting in a nearly simultaneous ignition in the discharge volume.

Sun et al. [8] showed that *in situ* generated nanosecond plasma had a significant effect on ignition-extinction characteristics of CH_4/He/O_2 counterflow diffusion flames, replacing the conventional S-curve with a new monotonic stretched ignition curve. In general, due to the complexity of the interaction between plasma and flame kinetics, the fundamental enhancement mechanisms are poorly understood.

Recently, Li et al. [11] developed a burner platform to study the coupling between laminar, low-pressure, premixed flames and *in situ* generated nanosecond plasma discharges. The combination of diffuse plasma and a steady, laminar, quasi-one-dimensional flame in this configuration is conducive to both laser-based measurements and numerical modeling with detailed kinetic mechanisms. In the present work, we investigate the effect of pulsed nanosecond discharges on a lean (ϕ = 0.5), premixed H_2/O_2/N_2 flame operating at 25 torr with the burner platform described in [11]. Spatially-resolved OH and temperature measurements are performed with and without a burst of 200 discharge pulses. A self-consistent, one-dimensional numerical model [4, 12] capable of resolving electric field transients over nanosecond timescales (during each discharge pulse) and radical kinetics and transport

processes occurring at micro-to-millisecond timescales is used to develop insight into the complex plasma/flame interactions. A particular focus is given to understand the role of thermal vs kinetic effects of the plasma on the laminar premixed flame.

2. Experimental Details

2.1 Plasma-Flame Facility

The plasma-flame facility has been described in detail previously [11], so only a brief overview is given here. Briefly, a water-cooled, 6-cm-diameter McKenna burner [13] is housed within a low-pressure chamber (Fig. 1a) capable of achieving stable (combusting) operating conditions down to 5 torr. The McKenna burner produces a steady, laminar, quasi-one-dimensional flame, which is conducive to both laser-based measurements and numerical modeling with detailed kinetic mechanisms. The flow rates of the gases are monitored by calibrated mass flow controllers and the total pressure within the chamber is maintained at a pressure of 25 Torr by a throttled vacuum pump (Welch 1397). In addition, the entire burner facility can be translated in the vertical direction with a resolution of 3 μm to facilitate spatially-resolved laser-based measurements as a function of height above the burner surface.

As shown in Fig. 1b, the configuration referred to as "direct flame coupling" (DFC) is investigated, which consists of encapsulating the "entire" combustion process (preheating, high-temperature reaction zone, and products) within the plasma discharge. The burner surface acts as the ground electrode, and the high-voltage electrode is a 12-cm-diameter Tungsten mesh (open area = 90%) located 40 mm above the burner surface, which is supported by four ceramic posts mounted to the outer portion of the McKenna burner (see Fig. 1b). This location of the high-voltage electrode results in direct coupling of the plasma processes to the combustion chemistry of interest, while providing minimal disturbance to the laminar flow field. As shown in [11], the uniformity of the large-volume plasma discharge under the low-pressure and high-temperature conditions of the plasma-flame facility is quite good.

2.2 OH Laser-Induced Fluorescence Measurements

Figure 2 shows a schematic of the OH LIF diagnostic system which is used to measure temperature and quantitative OH mole fractions in the low-pressure plasma/flame facility. A digital delay generator (Stanford Systems DG 645) serves as the "master clock" for the entire system sending a 10 Hz signal to both an Nd:YAG laser system and the nanosecond-pulsed plasma generator such that the LIF measurement is synchronized to the plasma discharge. The second harmonic output of an Nd.YAG laser (Spectra-Physics Indi-40-10) operating at 532 nm is used to pump a tunable, dye laser (Sirah Cobra-Stretch) to generate wavelengths in the vicinity of 562 nm. The visible output near 562 nm is frequency-doubled using a type-I BBO crystal to generate tunable ultraviolet output near 281 nm, which can excite the (1,0) band of OH $A^2\sum^+ - X^2\Pi$ system. The combination of a half wave plate and a thin film polarizer is used to attenuate the laser energy to less than 0.4 μJ/pulse to avoid saturation of the excited transitions. The UV laser beam then passes through a 500 μm-diameter pin hole, which defines the spatial resolution of the measurements in the direction normal to laser propagation, and passes into the vacuum chamber through a fused silica laser window oriented near Brewster's angle to minimize reflections.

For low laser pulse energies, the fluorescence signal is expressed as

$$S_{fl} = n_{OH} \frac{B_{12}}{c} \frac{E}{\Delta \nu_L} f_B \Gamma \phi F_{fl} l \frac{\Omega}{4\pi} \varepsilon \eta \tag{1}$$

where n_{OH} is the number density of OH; B_{12} is the Einstein absorption coefficient; c is the speed of light; E is the laser energy; $\Delta\nu L$ is the laser linewidth; f_B is the Boltzmann fraction; Γ is the dimensionless overlap integral between the laser and the absorption lineshapes; ϕ is the fluorescence quantum yield; F_{fl} is the fraction of fluorescence bandwidth collected; l is the laser path length sampled by the collection optics; ε is the efficiency of the optical system; and η is the efficiency of the detection system. The fluorescence emitted from the center of the flame is collected and focused onto a photo-multiplier tube (PMT; Hamamatsu R9220) by a set of two plano-convex spherical lenses. Schott glass BG3 and UG11 optical filters are placed in front of the PMT in order to block the broadband flame and plasma emission and allow collection of the OH LIF emission only. The

individual pulse-to-pulse energy fluctuations are monitored with a fast-response photodiode (Thorlabs DET10A; rise time of 1 ns). Both the OH fluorescence signal and the relative laser energies (photodiode signals) are collected on a digital oscilloscope (Lecroy Wave Runner 104Xi-A; 1 GHz bandwidth). When determining quantitative OH measurements from measured LIF signals, the fluorescence quantum yield is determined as $\phi = \tau_{fl}/\tau_{rad}$, where τ_{fl} is the measured fluorescence lifetime and τ_{rad} is the collision-free, radiative lifetime. The fluorescence lifetime is determined by fitting the measured fluorescence signal to a single exponential decay and the radiative lifetime is taken from German [14]. For the spatially-resolved measurements, only one time delay (Δt=8 μs) between the plasma discharge and the Nd:YAG laser is reported. This Δt corresponds to the time delay after which the largest increase of OH (due to the presence of the plasma) is measured and the plasma emission (e.g., N2(C-B)) had completely decayed.

Spatially-resolved temperature profiles were measured by recording OH LIF profiles for five rotational states, R1(8), R1(9), R1(10), R1(11), R1(13), of the OH $A^2\sum^+ \leftarrow X^2\prod$ (v'=1, v''=0) transition. For each spatial position (in 500 μm steps), the measured intensity was plotted against the rotational energy in a Boltzmann plot to determine the temperature. Two hundred laser shots (and hence fluorescence waveforms) were recorded at each location. The relative OH LIF signals from the R1(9) rotational line were converted to relative OH mole fraction profiles by correcting the LIF signals for pulse energy, temperature, Boltzmann fraction, and overlap integral variations as a function of height above the burner. The relative OH mole fraction profiles were placed on an absolute scale by normalizing the profiles by a LIF measurement in a well-characterized ϕ = 1.07 $CH_4/O_2/N_2$ flame at a height of 1.2 cm above the burner surface. For the absorption measurement, the laser system was tuned to the Q1 (10) rotational line within OH $A^2\sum^+ \leftarrow X^2\prod$ (v'=0, v''=0) transition near 309.5 nm and the measured mole fraction of 0.0104 is within 7% of previously-published results in the same flame [15].

The uncertainty of the temperature measurements is primarily due to finite signal-to-noise ratio (SNR) considerations. Lower SNR of high rotational levels introduces a 10% (+/-100K) uncertainty at low temperatures (800-1000 K). At temperatures greater than 1000 K, the uncertainty decreases to approximately 3% (+/-50K). To

a large extent, we avoid the temperature influence on OH measurements by using line R1(9). Quantification of the OH LIF signal, however, requires several temperature-dependent considerations including the Boltzmann population, electronic quenching due to other species, and the overlap of the laser frequency with the Doppler-broadened OH absorption transition. Uncertainty is also introduced when the relative OH profiles are placed on an absolute scale using direct absorption. All of these considerations lead to an estimated uncertainty of 20% in the absolute OH concentration measurements.

3. Numerical Framework

In order to obtain more insight into the multi-scale interactions between the laminar flame and nanosecond pulsed discharges, one dimensional, self-consistent simulations are performed with detailed chemistry. The details of the numerical framework are described elsewhere [4, 12]. Briefly, equations for electric potential, electron energy, and charged and neutral species continuity are considered. In addition, continuity, momentum and gas temperature equations are solved. The electron transport and reaction coefficients are expressed as functions of electron energy using predictions of a Boltzmann equation solver BOLSIG [16], and updated at every timestep through interpolation. The mixture-averaged formulation from CHEMKIN package [17] is used to obtain thermal conductivities and diffusion coefficients.

A non-uniform mesh consisting of 600 grid points is used to obtain grid converged solutions, with high resolution near the flame location and close to the electrodes. Temperature, velocity, and species mole fractions are specified at the inlet. Vanishing gradient boundary condition is applied for the energy equation, whereas species mole fractions are extrapolated at the outlet. Charged species fluxes include a drift component (due to electric field), and electron flux at the cathode boundary has contribution from secondary emission.

A simulation is performed at 25 torr with the discharge pulser switched off (no plasma) to obtain a steady-state flame solution shown in Fig. 3. Mole fractions of H_2, O_2 and N_2 at the inlet are 0.2327, 0.2327 and 0.5346 respectively (obtained from the experimental operating conditions). The temperature and velocity at the inlet are fixed at T_{in} = 345 K and u_{in} = 0.36 m/s respectively. Spatially-resolved OH and temperature data from the

experiments, also shown in Fig. 3, compare well with the predictions, validating the transient flame model without the plasma. The flame solution provides initial neutral species and temperature distributions for the pulsed discharge simulations. The charged species mole fractions are initialized to 1×10^{-10}, except for electron density fraction, which is initially fixed at 6×10^{-10} to ensure charge neutrality. Owing to the pulsed nature of the discharge process considered in this work, photoionization is not important and residual electrons from previous pulses provide seed electrons for initiation of the next pulse. The predictive capability of the present numerical code has been validated previously for pulsed nanosecond discharges in air [12] and H_2-air mixtures [4].

3.1 $H_2/O_2/N_2$ Plasma Flame Chemistry

A detailed kinetics mechanism consisting of 42 species and 310 reactions was compiled by combining $H_2/O_2/N_2$ plasma chemistry data [18-19] with conventional H_2-O_2 combustion kinetics [19-20] and NO_x kinetics [21-22]. The mechanism incorporates charged species O^+, N_2^+, O_2^+, N_4^+, O_4^+, H_2^+, H_3^+, HN_2^+, HO_2^+, H_2O^+, H_3O^+, O^-, O_2^-, and e^-, excited species $N_2(A^3\Sigma)$, $N_2(B^3\Pi)$, $N_2(C^3\Pi)$, $N_2(a'^1\Sigma)$, $N(^2D)$, $O_2(a^1\Delta)$, $O_2(b^1\Sigma)$, $O_2(c^1\Sigma)$, and $O(^1D)$; neutral species N_2, H_2, O_2, H, O, N, O_3, OH, HO_2, H_2O_2, H_2O, NO, NO_2, NH, NNH, NH_2, NH_3, N_2O and HNO. The plasma chemistry processes pertaining to H_2O (ionization, dissociation etc.) have also been included since they are important in accurately predicting the discharge development downstream of the flame. The present model does not incorporate vibrational excitation by electron impact and vibrational energy transfer processes. Our previous results [4] demonstrated that vibrational non-equilibrium in plane-to-plane nanosecond pulse discharges in air and H_2-air is insignificant.

4. Results and Discussion

The experiments make use of a high-voltage, short duration fast ionization dynistor (FID) plasma generator. Voltage and current pulse shapes during pulser operation were measured with a Tektronix P6015A high-voltage probe and Pearson (model 2877) current monitor and are shown in Fig. 4. The pulse width, as defined by the full width at half maximum (FWHM) value, is approximately 7 ns and the estimated pulse energy is 3 mJ/pulse,

which is independent of the flame conditions. We observe a delay between the voltage and the current, with the latter achieving a peak value of ~60 A, nearly 6 ns after the voltage reaches its maximum value. The corresponding curve-fit to the FID voltage waveform used in the simulations, and the calculated current are also shown in Fig. 4. As shown in Fig. 4, the model is able to accurately predict the shape of the current pulse, although it under-predicts the peak value by 20%. The predicted coupled energy is 3.4 mJ per pulse, which is close to the value calculated from the voltage and current measurements.

Figure 5 shows the model predictions of electron number density and reduced electric field (E/N) as a function of space and time during a discharge pulse in presence of a lean, premixed $H_2/O_2/N_2$ flame. The inlet conditions and initial flame conditions (i.e., without plasma) are the same as in Fig. 3. The E/N profiles are similar to that of temperature, with lower values in the pre-heat zone because of higher number density. The E/N attains much higher values (up to 1500 Td) for a short duration near the right boundary because of the cathode sheath formation. A significant portion of the input energy is expended to electron impact ionization in the high-temperature, post-flame gases because of high E/N (700-1000 Td). Due to the lower temperatures near the burner and in the preheating zone, input energy is coupled at E/N values of 100-700 Td, resulting in efficient generation of radicals and excited species via electron impact dissociation and excitation processes, as well as quenching of excited electronic states of N_2. The electron density evolves in a spatially-uniform manner with a peak value of ~7×10^{12} cm^{-3} attained at ~21 ns.

Figure 6(a) shows spatially-resolved OH density and temperature measurements as a function of height above the burner surface, with and without the application of 200 discharge pulses at a 40-kHz repetition rate. A significant increase in OH concentration is observed after the pulse burst, with a 40% increase in the peak mole fraction from 0.003 to 0.004 at 2 cm location above the burner. The plasma effect also results in approximately 20% rise in temperature in the burnt gas region. While the temperature rise in the preheat zone (0.5 cm to 1.5 cm above the burner surface) is similar (20%), the increase in OH mole fraction is substantially higher. For example,

the OH mole fraction increases from 0.001 to 0.0025 9 mm above the burner surface, which corresponds to an increase of 140%. Larger increases are observed closer to the burner surface.

Numerical simulations were performed to gain further insight into the plasma flame interactions. A burst of 200 FID pulses applied at 40 kHz repetition rate were simulated at the same operating conditions as in the experiments. The predicted temperature and OH profiles with and without the burst of 200 pulses are also shown in Fig. 6(a). The inlet conditions and initial flame conditions (i.e., without plasma) are the same as in Fig. 3. The model performs well in predicting the OH mole fraction and temperature rise in the pre-heat zone. In the burnt-gas regions, OH concentration is over-predicted, whereas the calculated temperatures are ~10% below the measured values. However, the trend is correctly predicted in both cases, giving confidence in utilizing the model framework to investigate the plasma and flame interactions.

Figure 6(b) shows the spatial distribution of O and H radicals predicted by the model at various points in time during the 200 pulse simulation. A significant rise in species concentrations is observed because of the pulsed discharge processes, with peak values of H and O increasing by approximately a factor of 4 and a factor of 6, respectively. It is interesting to note that the gradients of radical concentrations and temperature are substantially higher in the pre-heat zone from the plasma energy addition. This suggests that the plasma chemistry accelerates ignition, resulting in the species concentration profiles moving upstream by approximately 0.2 cm. Figure 7 shows a path flux analysis quantifying the key production pathways of O, H and OH at 0.6 cm location above the burner. A substantial fraction of O and H radicals are generated directly by dissociation of O_2 and H_2 molecules through collisions with high-energy electrons (electron impact) and excited N_2 species (dissociative quenching). On the other hand, OH is a secondary radical generated by reactions of O and H with HO_2, in addition to other chain-branching reactions. Note that OH produced by the pulsed plasma triggers heat release by reactions of OH with H_2, to generate H_2O and H. The resultant increase in temperature accelerates the conventional H_2 - O_2 chain branching processes, thereby creating a positive feedback loop for rapid production of radicals. At locations closer to the burner, lower temperatures aid in the formation of O_3 and HO_2 from O and H radicals, respectively. Ozone

is transported a short distance downstream before it decomposes to O when the temperature rises above 500 K. HO_2 persists for a longer distance until the temperature increases to about 700 K.

In the present configuration, the time-averaged discharge power during the burst is nearly 50% of the heat of combustion. Thus, it is not surprising that the pulsed plasma source has a significant impact on flame properties. It is, however, critical to understand if the plasma effect is predominantly thermal, or if non-equilibrium kinetics play an important role in modifying the flame structure. To determine this, we performed an additional simulation, considering only the Joule heating effect during each pulse and with the electron impact chemistry processes switched off. The Joule heating term is given by the following equation,

$$J_H = \left| e\vec{E}.(\vec{\Gamma}_+ \quad \vec{\Gamma}_- \quad \vec{\Gamma}_e) \right| \tag{2}$$

where $\vec{E}$ is the electric field, $\vec{\Gamma}_+$, $\vec{\Gamma}_-$, and $\vec{\Gamma}_e$ are the fluxes of positive ions, negative ions, and electrons, respectively, and e the electron charge. This quantity was calculated as a function of space and time from electric field and flux data predicted by the pulsed discharge simulation in Fig. 6. J_H is used as a source term in the gas temperature equation, while all electron impact processes during the discharge pulses are turned off. Figure 8 shows spatial distributions of temperature as well as O, H, and OH number densities after a burst of 200 discharge pulses with and without incorporating electron impact kinetics (in the latter case, only Joule heating is incorporated). The peak values of O and H densities decrease by nearly 30% when the non-equilibrium electron chemistry effects are not taken into account in the model. As seen in Fig. 6, adding pulsed plasma results in O and H densities increase by a factor of 4 and 6, respectively. We can therefore conclude that Joule heating is responsible for a significant fraction of the plasma enhancement of the flame. Non-equilibrium chemistry effects, however, are of critical importance in the lower-temperature regions upstream of the flame. It is evident that species and temperature gradients are less steep when only Joule heating effect is considered. Also, adding all discharge energy in form of heat results in 20% lower temperature compared with the case considering non-equilibrium chemistry effects. The difference in temperature can be attributed to the heat release triggered by partial oxidation of fuel molecules by the plasma-generated radicals. Joule heating alone cannot move the

temperature and species profiles as far upstream (i.e. closer to the burner surface) as the pulsed plasma source of the same total power.

Future work will focus on techniques to increase the energy coupled in the pre-heat zone through the use of upstream plasma configuration [11], and understanding the plasma and premixed flame interactions for hydrocarbon fuels.

5. Conclusion

A novel plasma-flame facility has been developed to study the direct coupling of steady, laminar, low-pressure, premixed flames to highly non-equilibrium, nanosecond-pulsed plasma discharges. OH LIF diagnostics was used to measure temperature and quantitative OH mole fraction profiles, with high spatial resolution. The measurements were performed with and without a burst of 200 nanosecond discharge pulses to quantify the effect of non-equilibrium plasma on a pre-existing lean premixed $H_2/O_2/N_2$ ($\phi = 0.5$) flame. Temperature increased by approximately 20% at all spatial locations and OH mole fraction increased by 100-500 % in the preheat region and 40% in the post-flame gases due to the application of discharge pulses. A one-dimensional, multi-scale, pulsed discharge modeling framework with detailed plasma combustion kinetics was used to develop additional insight into the complex plasma- flame interactions. Simulation results showed a significant increase in O and H densities due to plasma chemistry, with peak values increasing by a factor of 6 and a factor of 4, respectively. Additional simulations were conducted considering only Joule heating, to compare the thermal effect vs kinetic (plasma chemistry) effect. Joule heating was found responsible for a significant fraction of the plasma enhancement of the combustion processes, although electron impact processes were shown to play an important role in radical production and heat release in the pre-heat zone. It was demonstrated that Joule heating alone cannot move the temperature and species profiles as far upstream (i.e. closer to the burner surface) as the pulsed plasma source of the same total power.

Acknowledgements

This work was supported by the MURI research grant FA9550-07-1-0136 from the Air Force Office of Scientific Research with Dr. Chiping Li as the technical monitor.

References

[1] S. M. Starikovskaia, J. Phys. D: App. Phys. 39 (16) (2006) R265-R299.
[2] Y.P. Raizer, Gas Discharge Physics, Springer, Barcelona, Spain, 1991.
[3] Z. Yin, I. V. Adamovich, and W. R. Lempert, Proc. Combust. Inst. 34 (2013) 3249-3258.
[4] S. Nagaraja, V. Yang, Z. Yin, and I. V. Adamovich, Combust. Flame (2013)
[5] I. N. Kosarev, N. L. Aleksandrov, S. V. Kindysheva, S. M. Starikovskaia, and A. Yu Starikovskii, Combust. Flame 156 (1) (2009) 221-233.
[6] C. D. Cathey, T. Tang, T. Shiraishi, T. Urushihara, A. Kuthi, and M. A. Gundersen, IEEE Trans. Plasma Sc. 35 (6) (2007) 1664-1668.
[7] T. Ombrello, S.H. Won, Y. Ju, S. Williams, Combust. Flame 157 (2010) 1906-1915.
[8] W. Sun, S. H. Won, T. Ombrello, C. Carter, and Y. Ju, Proc. Combust. Inst. 34 (1) (2013) 847-855.
[9] G. Pilla, D. Galley, D.A. Lacoste, F. Lacas, D. Veynante, C.O. Laux, IEEE Trans. Plasma Sci. 34(6) (2006) 2471-2477.
[10] W. Kim, M.G. Mungal, M.A. Cappelli, Combust. Flame 157(2) (2009) 374-383.
[11] T. Li, I.V. Adamovich, J.A. Sutton, Combust. Sc. Tech. 185 (2013) 990-998.
[12] S. Nagaraja, V. Yang, and I. V. Adamovich, J. Phys. D: App. Phys. 46 (15) (2013) 155205.
[13] HOLTHUIS & ASSOCIATES at <www.flatflame.com>.
[14] K.R. German, J. Chem. Phys. 63 (1975) 5252.
[15] P.A. Berg, D.A. Hill, A.R. Noble, G. P. Smith, J.B. Jeffries, and D.R. Crosley, Combust. Flame 121 (2000) 223-235.
[16] G. J. M. Hagelaar and L. C. Pitchford. Plasma Sour. Sc. Tech. 14 (4) (2005) 722.
[17] R. J. Kee, J. F. Grcar, M. D. Smooke, and J. A. Miller, PREMIX: a Fortran program for modeling steady laminar one-dimensional premixed flames, Sandia National Laboratories Report, 1985
[18] M. Uddi, N. Jiang, I. V. Adamovich, and W. R. Lempert. J. Phys. D: App. Phys. 42 (7) (2009) 075205.
[19] N. A. Popov. *Plasma Phys. Rep.* 34 (5) (2008) 376-391.
[20]A. A. Konnov, *Combust. Flame* 152 (4) (2008) 507-528.
[21] G.P.Smith, D.M.Golden, M.Franklach, et al. GRI-Mech 3.0 (1999), available at http://www.me.berkeley.edu/gri_mech/
[22] K. Takita, N. Abe, G. Masuya, and Y. Ju, Proc. Combust. Inst. 31 (2) (2007) 2489-2496.

Fig. 1 – (Left to right) (a) Photograph of plasma-flame facility; (b) photograph of McKenna burner and high-voltage electrode; (c) schematic of the "Direct Coupling" configuration.

Fig. 2 – Schematic of the coupled OH laser induced fluorescence system and low-pressure plasma/flame facility.

Figure 3: Steady-state temperature and species concentration distributions as functions of height above the burner for a $H_2/O_2/N_2$ ($\phi = 0.5$) flame at 25 torr, with plasma discharge switched off.

Figure 4: FID voltage and current waveforms measured at the high voltage electrode; voltage curve-fit used in the simulations and predicted current at 25 torr in a $H_2/O_2/N_2$ ($\phi = 0.5$) flame.

Figure 5: Spatial distributions of reduced electric field, E/N, and electron number density during a FID voltage pulse predicted by the model at 25 torr in a $H_2/O_2/N_2$ ($\phi = 0.5$) flame.

Figure 6: (a) Measured and predicted OH mole fraction and temperature distributions, (b) predicted O and H number densities as a function of height above burner before and after a burst of 200 FID pulses at 25 torr in a $H_2/O_2/N_2$ ($\phi = 0.5$) flame.

Figure 7: Path flux analysis describing the major formation/destruction pathways of (a) O, (b) H and OH after a burst of 200 FID pulses at 0.6 cm location above the burner at 25 torr in a $H_2/O_2/N_2$ ($\phi = 0.5$) flame. Percentage contributions of difference channels are indicated.

Figure 8: Predicted O, H, and OH densities and temperature distributions as functions of height above the burner after a burst of 200 FID pulses, with and without incorporating electron impact kinetics into the model at 25 torr in a $H_2/O_2/N_2$ ($\phi = 0.5$) flame.

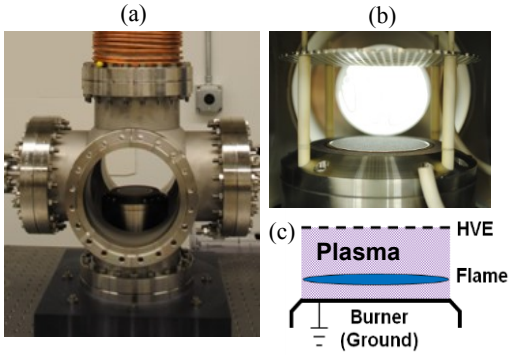

Fig. 1 – (Left to right) (a) Photograph of plasma-flame facility; (b) photograph of McKenna burner and high-voltage electrode ; (c) Concept of the “Direct Coupling” configuration.

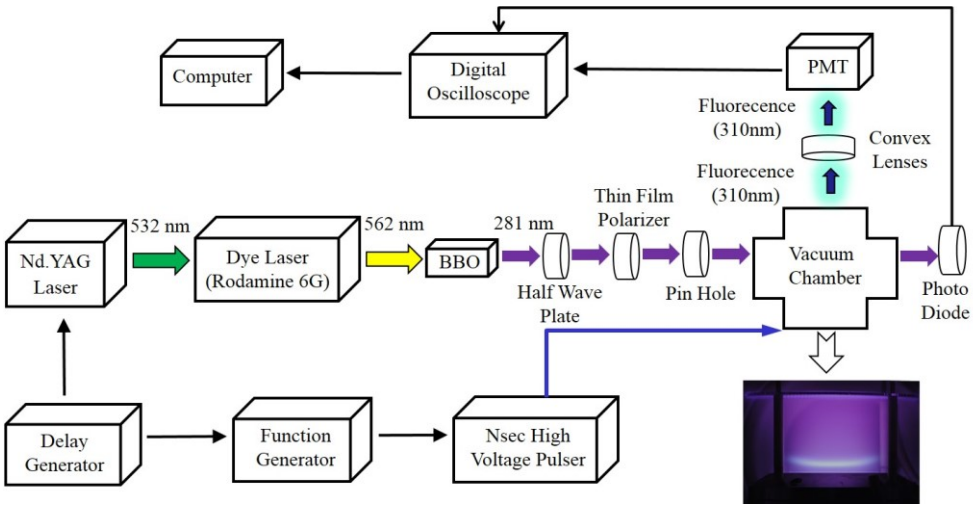

Fig. 2 – Schematic of the coupled OH laser -induced fluorescence system and low-pressure plasma/flame facility

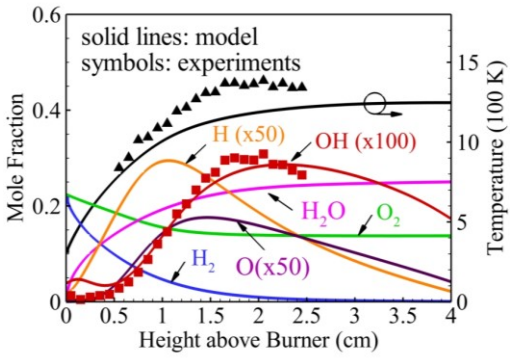

Figure 3: The steady-state temperature and species concentrations as a function of height above burner with discharge source switched off at 25 torr for a $H_2/O_2/N_2$ ($\phi = 0.5$) flame.

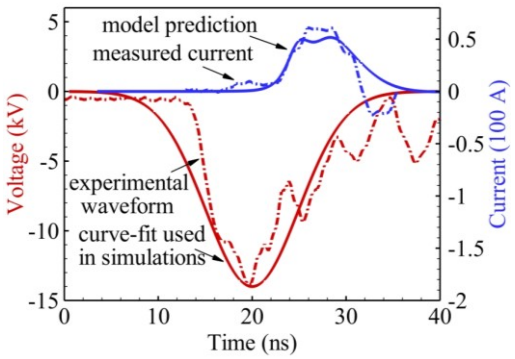

Figure 4: FID waveform applied at the high voltage electrode and the curve-fit used in the simulations, along with the measured and predicted current at 25 torr in a $H_2/O_2/N_2$ ($\phi = 0.5$) flame.

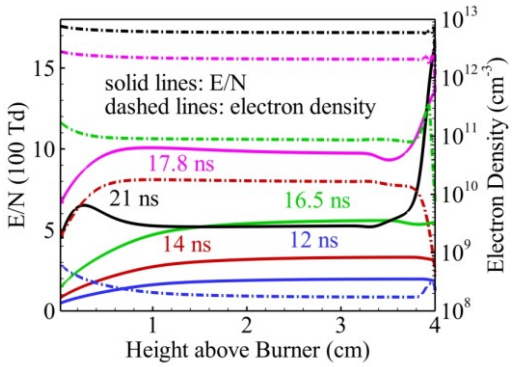

Figure 5: Spatial distributions of reduced electric field, E/N and electron number density during a FID voltage pulse predicted by the model at 25 torr in a $H_2/O_2/N_2$ ($\phi = 0.5$) flame.

(a)

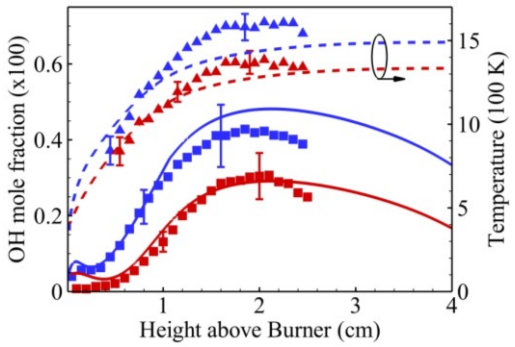

(b)

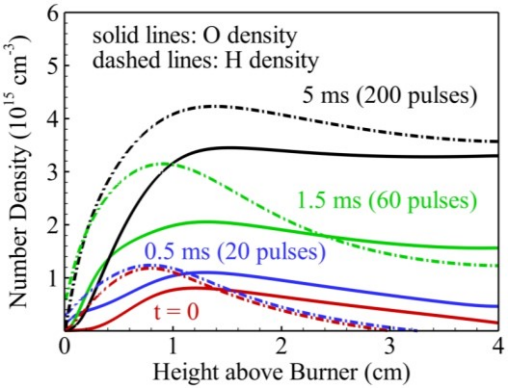

Figure 6: (a) Measured and predicted OH concentration and temperature, (b) predicted O and H densities as a function of height above burner before and after a burst of 200 FID pulses at 25 torr in a $H_2/O_2/N_2$ ($\phi = 0.5$) flame.

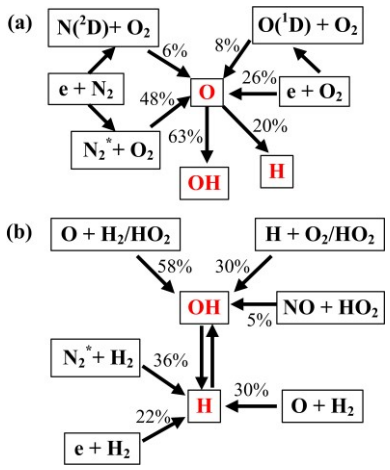

Figure 7: Path flux analysis describing the major formation/destruction pathways of (a) O, (b) H and OH after a burst of 200 FID pulses at 0.6 cm location above the burner at 25 torr in a $H_2/O_2/N_2$ ($\phi = 0.5$) flame.

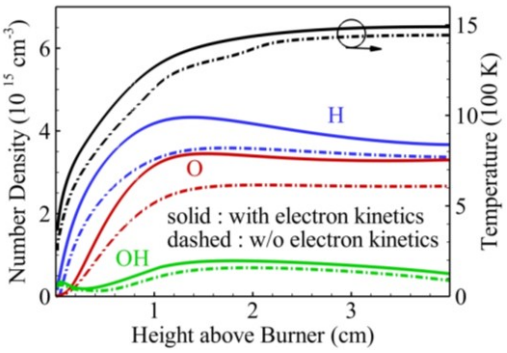

Figure 8: Predicted O, H, OH densities and temperature as a function of height above burner after a burst of 200 FID pulses with and without considering electron impact kinetics in the model at 25 torr in a $H_2/O_2/N_2$ (ϕ = 0.5) flame.